Full-Color Emission from In_2S_3 and In_2S_3:Eu^{3+} Nanoparticles

Wei Chen,*,† Jan-Olov Bovin,‡ Alan G. Joly,§ Shaopeng Wang,† Fuhai Su,¶ and Guohua Li¶

Nomadics, Inc., 1024 South Innovation Way, Stillwater, Oklahoma 74074, Department of Materials Chemistry, Chemical Center, University of Lund, S-22100, Lund, Sweden, Pacific Northwest National Laboratory, P.O. Box 999, Richland, Washington 99352, and National Laboratory for Superlattices and Microstructures, Institute of Semiconductors, Chinese Academy of Sciences, P.O. Box 912, Beijing 100083, China

Received: May 2, 2004; In Final Form: June 2, 2004

New observations on the luminescence of In_2S_3 and europium-doped In_2S_3 nanoparticles show a green (510 nm) emission from In_2S_3 and $In_{1.8}Eu_{0.2}S_3$ nanoparticles while a blue (425 nm) emission is observed from $In_{1.6}Eu_{0.4}S_3$ nanoparticles. Both the blue and green emissions have large Stokes shifts of 62 and 110 nm, respectively. Excitation with longer-wavelength photons causes the blue emission to shift to a longer wavelength while the green emission wavelength remains unchanged. The lifetimes of both the green and blue emissions are similar to reported values for excitonic recombination. When doped with Eu^{3+}, in addition to the broad blue and green emissions, a red emission near 615 nm attributed to Eu^{3+} is observed. Temperature dependences on nanoparticle thin films indicate that with increasing temperature, the green emission wavelength remains constant, however, the blue emission shifts toward longer wavelengths. Based on these observations, the blue emission is attributed to exciton recombination and the green emission to Indium interstitial defects. These nanoparticles show full-color emission with high efficiency, fast lifetime decays, and good stability; they are also relatively simple to prepare, thus making them a new type of phosphor with potential applications in lighting, flat-panel displays, and communications.

1. Introduction

Luminescent materials or phosphors can be found in a broad range of everyday applications such as cathode ray tubes, projection television screens, fluorescent tubes, X-ray detectors, and biomedical probes.[1] Efforts over the last three decades have led to phosphor materials that operate close to their physical limits.[1] Thus, it cannot be expected that properties such as quantum efficiency and spectral energy distribution will be significantly improved or that distinctly better materials will be found in the near future. However, the present phosphors have some shortcomings that need to be addressed. For example, Zn_2SiO_4:Mn^{2+} (willemite) is used as a green phosphor because its green emission color is extremely saturated. However, its luminescence decay lifetime is rather long, tens of milliseconds.[1] In applications involving fast-moving images, this causes a green afterglow that can blur the display. As a result of quantum size confinement,[2] nanoscale phosphors may offer significant improvements compared with conventional bulk phosphors. Luminescent nanoparticles may have an increase in electron−hole overlap, thus yielding greater oscillator strength and an enhancement of luminescence quantum efficiency.[3] Since the emission decay lifetime is inversely proportional to the oscillator strength of a transition,[4] the lifetime is shortened with decreasing size. Thus, high efficiencies with short decay times make nanoparticles a new type of luminescent material with potential applications.[5]

As a new type of luminescent material, II−VI semiconductor nanoparticles such as CdTe and CdSe have received much attention.[6] However, much less work has been performed on III−VI semiconductor nanoparticles such as In_2S_3.[7−12] One of the advantages of In_2S_3 over other III−V semiconductors such as InP, InAs, and GaAs is that In_2S_3 can be synthesized from solution by chemical methods while sophisticated techniques such as molecular beam epitaxy are needed for fabricating other III−V semiconductors. The preparation of In_2S_3 from an aqueous solution of $InCl_3$ using H_2S,[7,12] Na_2S,[8,10] CS_2,[9] and CH_3CSNH_2[11] have been reported. Absorption spectra, photochemical kinetics, and photosensitization effects have been reported in In_2S_3 nanoparticle colloids.[7−12] These results indicate that In_2S_3 nanostructured materials or thin films may find potential applications as solar cell materials. Nagesha et al.[8] reported the luminescence of In_2S_3 nanoparticles with emission at 360−380 nm and a quantum yield of 1.5% and Xiong et al.[9] have prepared In_2S_3 nanophase dendrites with an emission peaking at 358 nm. These UV emissions have been assigned to the excitonic or band-to-band transitions of In_2S_3 nanoparticles.[8,9] An orange emission at 600 nm from In_2S_3 nanoparticles embedded in sol−gel silica xerogel was reported and attributed to the luminescence from In^{3+} ions.[10] We have observed that small quantities of metallic ions such as europium in the preparation solutions helps to control the particle size and passivate the particle surfaces. In this way, we have successfully synthesized In_2S_3 nanoparticles with high quantum efficiencies in the blue, green, and red spectral regions. In this paper, we discuss the structure, luminescence, and potential applications of In_2S_3 nanoparticles made using this novel recipe.

2. Experimental Details

The synthesis of indium-sulfide-doped nanoparticles is similar to the scheme of arrested precipitation used in the preparation of II−VI colloids with the exception that Mn^{2+} and Eu^{3+} ions

* Corresponding author: wchen@nomadics.com.
† Nomadics, Inc.
‡ University of Lund.
§ Pacific Northwest National Laboratory.
¶ National Laboratory for Superlattices and Microstructures.

10.1021/jp048107m CCC: $27.50
Published on Web 07/09/2004

are added to the solutions along with the chemical sources. Typically, 4 mL of 0.1 M $InCl_3$, 2 mL of 0.1 M $Mn(NO_3)_2$, and 0.5 mL of thioglycolic (mercaptoacetic) acid were dissolved in 50 mL of deionized water and degassed by N_2 bubbling for 20 min. For preparation of In_2S_3:Eu^{3+}-doped nanoparticles, calculated amounts of $Eu(NO_3)_3$ were mixed with the $InCl_3$. The pH's of the solutions were adjusted between 2.0 and 3.5. Each mixture was vigorously stirred and 6 mL of an 0.1 M aqueous solution of sodium sulfide was added. The solutions were refluxed for 5 h, after which the doped nanoparticles ($In_{1.8}Eu_{0.2}S_3$, $In_{1.6}Eu_{0.4}S_3$) formed. The procedure for the preparation of In_2S_3-undoped nanoparticles is the same except that no Eu^{3+} and Mn^{2+} ions were added to the precursor solution. We find that the particle size can be modified by adding ions such as Mn^{2+} and Eu^{3+} because metallic ions can inhibit the growth rate of the nanoparticles.

The structure, size, and elemental composition of the nanoparticles were determined by high-resolution transmission electron microscopy (HRTEM). The particles in solution were brought onto holey carbon (with holes)-covered copper grids for HRTEM observations. The HRTEM images of the particles were obtained with a JEM-3000F electron microscope (300 kV) with a structural information limit of 0.11 nm. The compositions of the particles were analyzed using an energy-dispersive X-ray spectrometer (EDS).

The optical absorption spectra were obtained on a Hewlett-Packard 8453 diode array spectrophotometer using 1-cm quartz cuvettes. Luminescence emission, excitation, and temperature-dependent luminescence were measured in a JY SPEX Fluorolog 3 Fluorometer. The quantum yield determination in this paper is the same as reported by Xiong et al.[9] The quantum yield was determined by comparing the luminescence with Rhodamine B in ethylene glycol (quantum yield near 100% at 580 nm). The optical densities of an In_2S_3 dispersion in water and the standard were adjusted to be within 0.05 absorbance units of each other at the excitation wavelength of 390 nm. The quantum yield was calculated according to the formula $\eta_{In_2S_3} = \eta_S (I_{In_2S_3}/I_S)^*(OD_S/OD_{In_2S_3})$, where $\eta_{In_2S_3}$ and η_S are the quantum yields of nanoparticles and standard, $I_{In_2S_3}$ and I_S are the integrated area of the luminescence peaks of the nanoparticles and the standard, and $OD_{In_2S_3}$ and OD_S are the optical densities of the nanoparticles and the standard at the excitation wavelength (390 nm). However, we note that the quantum yield measured in this way is not highly accurate as an absolute quantum yield, but gives reliable values for the relative quantum yields of the different particles. The purpose of measuring the quantum yield is to compare the fluorescence efficiencies of the samples of different sizes and to compare with published data in the literature. It is also noted that the quantum efficiency of Rhodamine B is excitation wavelength and solvent dependent. Its efficiency is largest in ethylene glycol (close to 100%), while in other solvents its yield is slightly lower. Recent measurements on In_2S_3 nanoparticles using both Rhodamine B and p-quaterphenyl as standards concluded that the quantum yield values obtained with the different standards were similar even though the emission wavelengths are quite different.[9] Therefore it is unlikely that the use of Rhodamine B as the quantum yield reference leads to significant quantitative errors, particularly in relative yield measurements.

The time-resolved spectral data were collected using a nanosecond optical parametric oscillator/amplifier (OPO) operating at a 10-Hz repetition rate and tunable between 220 and 1800 nm. The output was directed onto the particles and the emission was collected at right angles to the excitation and focused into a 1/8 m monochromator with a gated intensified CCD camera to record the time-resolved spectra. Picosecond lifetime data were collected using the output of a femtosecond amplified Ti:Sapphire laser operating at 1 kHz. The 150-fs, 760-nm output was frequency doubled in a 1 mm BBO crystal to provide excitation at 380 nm and directed onto the samples. The magic-angle polarized output emission was collected at right angles and focused into the entrance of a streak camera (Hamamatsu C5680). Appropriate filters were used to isolate the wavelengths of interest. The time resolution was determined to be 200 ps fwhm using a standard scattering material.

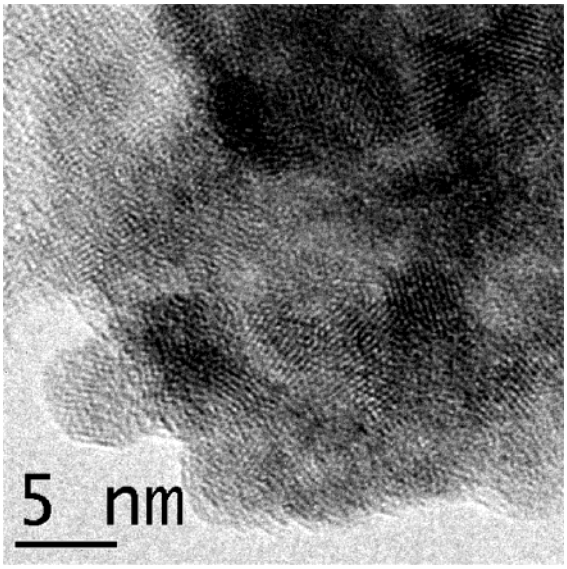

Figure 1. HRTEM images of deposited In_2S_3 nanoparticles showing a particles size of about 4 to 5 nm.

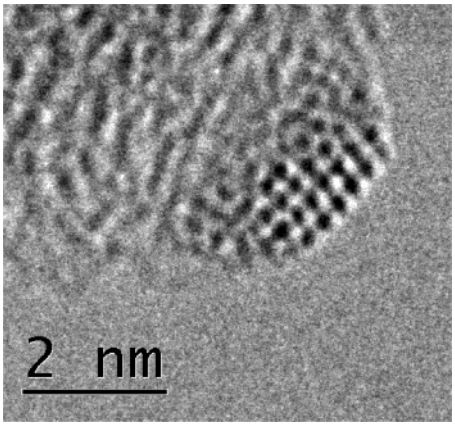

Figure 2. HRTEM images of deposited $In_{1.6}Eu_{0.4}S_3$ nanoparticles showing a particles size of about 2 to 3 nm.

3. Results

The In_2S_3 nanoparticles investigated with HRTEM (Figure 1) exhibit a cubic structure. The average size of the particles is in the range of 4 to 5 nm. The (111) lattice spacing of the particles is estimated to be around 0.3 nm from the HRTEM images, which is consistent with the (111) spacing of bulk In_2S_3,[13] indicating a cubic cell of 0.54 nm. HRTEM images (Figure 2) of the solution of $In_{1.6}Eu_{0.4}S_3$ particles show that the average size of the particles is around 2 to 3 nm in diameter. EDS analysis of aggregated particles such as the one in Figure 2 shows that the particles are composed of In, Eu, Mn, and S. (Figure 3). Clearly the Mn and Eu ions added in the preparation to inhibit particle growth are incorporated within or on the

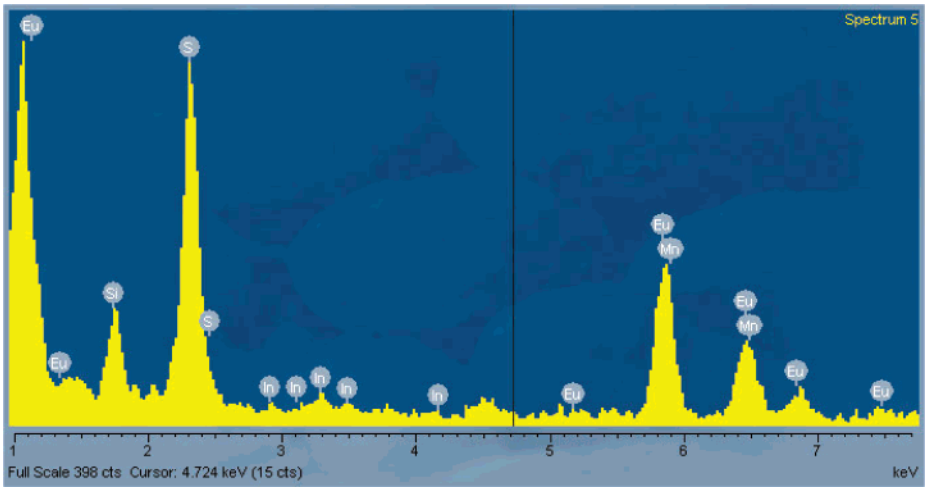

Figure 3. EDS analysis of an aggregate of $In_{1.6}Eu_{0.4}S_3$ nanoparticles, similar to the one in Figure 2. The analysis shows that the nanoparticles are composed of Eu, Mn, In, and S.

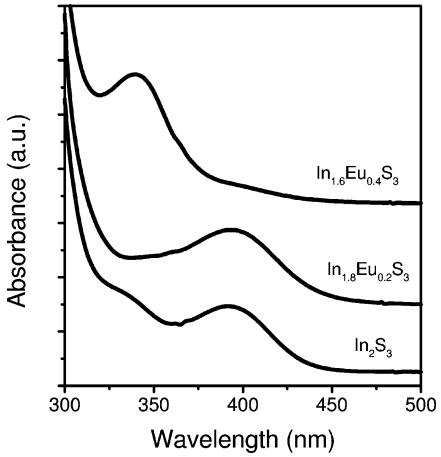

Figure 4. Absorption spectra of In_2S_3, $In_{1.8}Eu_{0.2}S_3$, and $In_{1.6}Eu_{0.4}S_3$ nanoparticles.

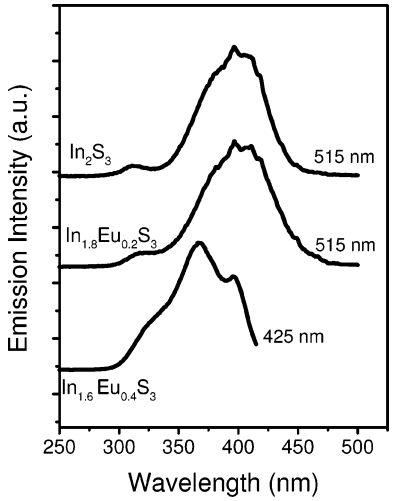

Figure 5. Excitation spectra of In_2S_3, $In_{1.8}Eu_{0.2}S_3$, and $In_{1.6}Eu_{0.4}S_3$ nanoparticles. The monitored emission wavelength is at 515 nm for In_2S_3 and $In_{1.8}Eu_{0.2}S_3$, and is at 425 nm for $In_{1.6}Eu_{0.4}S_3$ nanoparticles.

surface of the nanoparticles. The $In_{1.6}Eu_{0.4}S_3$ particles observed in the HRTEM images are most likely cubic close packed (ccp) with a cubic cell of about 0.54 nm. HRTEM observations and analysis confirm the formation of In_2S_3 nanoparticles in our preparation.

Figure 4 displays the absorption spectra of In_2S_3, $In_{1.8}Eu_{0.2}S_3$, and $In_{1.6}Eu_{0.4}S_3$ nanoparticles. For In_2S_3 and $In_{1.8}Eu_{0.2}S_3$ particles, a strong absorption peak is observed at 390 nm with a weak shoulder at 330 nm. For $In_{1.6}Eu_{0.4}S_3$ particles, a strong absorption peak is observed at 338 nm. Figure 5 displays the excitation spectra and Figure 6 shows the emission spectra of In_2S_3, $In_{1.8}Eu_{0.2}S_3$, and $In_{1.6}Eu_{0.4}S_3$ nanoparticles in aqueous solution. For In_2S_3 and $In_{1.8}Eu_{0.2}S_3$ nanoparticles, a strong green emission at 510 nm is observed while for $In_{1.6}Eu_{0.4}S_3$ particles a strong blue emission is observed at 425 nm. The quantum efficiencies for the green emission from In_2S_3, and $In_{1.8}Eu_{0.2}S_3$ are 1.6% and 2.2%, respectively. The quantum efficiency for the blue emission from $In_{1.6}Eu_{0.4}S_3$ is 33%. The efficiency from In_2S_3 nanoparticles is similar to that reported by Nagesha et al.[8] Interestingly, the efficiency from $In_{1.6}Eu_{0.4}S_3$ nanoparticles is one order of magnitude higher than that from pure In_2S_3 nanoparticles.

For In_2S_3 and $In_{1.8}Eu_{0.2}S_3$ particles, two absorption bands at 310 and 400 nm are observed in the excitation spectra. For $In_{1.6}Eu_{0.4}S_3$ particles, two absorption peaks are observed at 323 and 363 nm, respectively. The origins of the 310-nm peak in the excitation spectra of In_2S_3 and $In_{1.8}Eu_{0.2}S_3$ particles and the 323-nm shoulder in the excitation spectrum of $In_{1.6}Eu_{0.4}S_3$ nanoparticles are not clear. The main excitation band shifts to shorter wavelengths for $In_{1.6}Eu_{0.4}S_3$ nanoparticles compared with that of In_2S_3 and $In_{1.8}Eu_{0.2}S_3$ particles, likely due to increased quantum size confinement of the smaller particles. By comparing the absorption spectra with the excitation spectra, it is observed

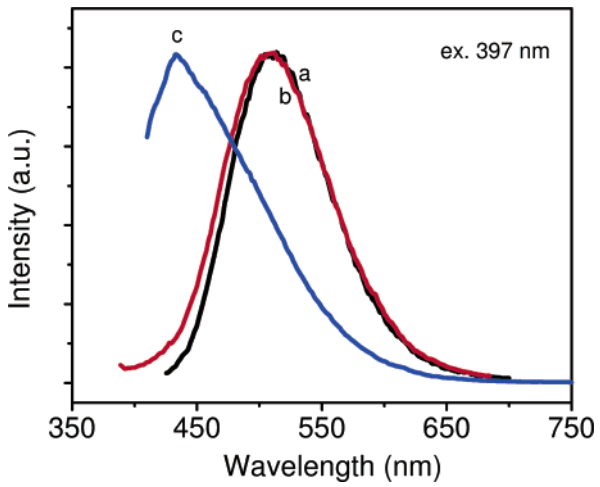

Figure 6. Emission spectra of In_2S_3 (a), $In_{1.8}Eu_{0.2}S_3$ (b), and $In_{1.6}Eu_{0.4}S_3$ (c) nanoparticles in aqueous solution following excitation at 397 nm.

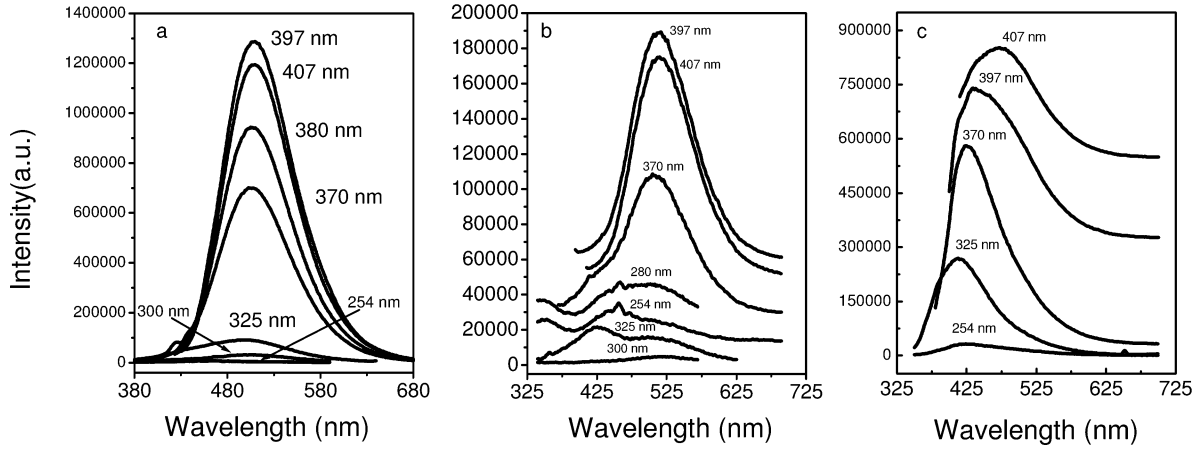

Figure 7. Emission spectra of In_2S_3 (a), $In_{1.8}Eu_{0.2}S_3$ (b), and $In_{1.6}Eu_{0.4}S_3$ (c) nanoparticle solutions at different excitation wavelengths as labeled in the spectra.

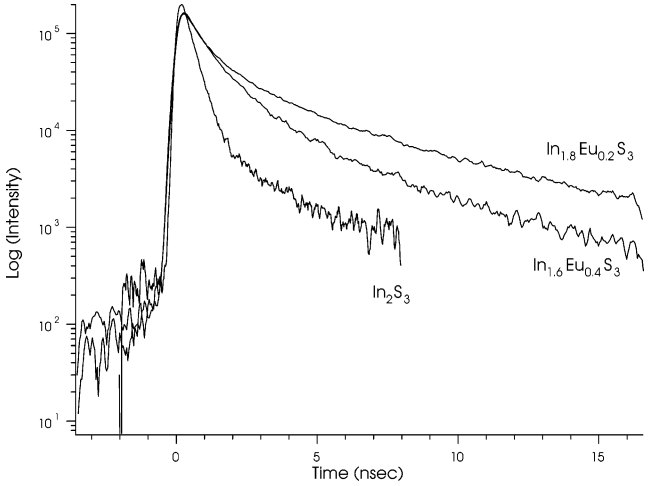

Figure 8. Luminescence lifetime decay curves of In_2S_3 (monitored at 500 nm), $In_{1.8}Eu_{0.2}S_3$ (monitored at 500 nm), and $In_{1.6}Eu_{0.4}S_3$ (monitored at 435 nm) nanoparticles following excitation at 380 nm.

that for each absorption band, the main peak in the excitation spectrum is at the absorption edge of the corresponding absorption peak in the absorption spectra. This is a common phenomenon in semiconductors since the photon-excitation rate is the greatest at the absorption edge where the absorption index is fairly low and the dispersion is small.[37]

Figure 7 displays the emission spectra of In_2S_3, $In_{1.8}Eu_{0.2}S_3$, and $In_{1.6}Eu_{0.4}S_3$ nanoparticle solutions at different excitation wavelengths. Figure 6 shows clearly that in In_2S_3 nanoparticles, the green emission position and shape do not vary significantly following excitation at different wavelengths. For $In_{1.8}Eu_{0.2}S_3$ nanoparticles, the green emission wavelength remains constant at different excitation wavelengths as well. However, a new emission peak at 425 nm appears following excitation at wavelengths shorter than 370 nm (Figure 6b). The blue emission at 425 nm is stronger in intensity than the green emission at 510 nm. Figure 6c shows the emission spectrum of $In_{1.6}Eu_{0.4}S_3$ following excitation at different wavelengths. The emission peak position moves to shorter wavelengths gradually as the excitation wavelength decreases.

Figure 8 shows the luminescence lifetime decays from In_2S_3, $In_{1.8}Eu_{0.2}S_3$, and from $In_{1.6}Eu_{0.4}S_3$ nanoparticles, near the peak wavelength of their respective emission following excitation at 380 nm. The lifetimes can be fit adequately with biexponential decay functions and the results of this fit are listed in Table 2. The decay lifetimes of the blue emission are about 700 ps and 2.5 ns while the green emission lifetimes depend on the sample with the shortest decay from the pure In_2S_3 particles. The longer nanosecond lifetime is slightly shorter than the excitonic luminescence decay lifetime previously observed in In_2S_3[8] and is similar to other semiconductor nanoparticles.[14]

4. Discussion

4.1. Luminescence of Indium Sulfide Nanoparticles in Solution. Table 1 summarizes the absorption and emission wavelengths of In_2S_3 and In_2S_3:Eu^{3+} nanoparticles in aqueous solution. For the green emission, the Stokes shift is around 110 nm, while for the blue emission, the Stokes shift is about 62 nm. The energy gap of bulk In_2S_3 is between 2.0 and 2.2 eV with the corresponding absorption edge from 620 to 550 nm.[15,16] In comparison, the absorption edge of the In_2S_3 nanoparticles is approximately 150−220 nm blue-shifted from bulk In_2S_3. This blue-shift is likely due to quantum size confinement. As the diameter of the semiconductor particle approaches the exciton Bohr diameter, its electronic properties change. The Bohr radius of the exciton in In_2S_3 may be calculated by[2,4]

$$a_B = \frac{\hbar^2 \epsilon}{e^2}\left[\frac{1}{m_e} + \frac{1}{m_h}\right] \quad (1)$$

where ϵ is the dielectric constant (~11), $\hbar$ is the Planck constant and m_e and m_h are the electron and hole effective mass, respectively. Assuming that $m_e = m_h = \mu = 0.25 \times 10^{-28}$ g,[12] the Bohr radius of the exciton in In_2S_3 is calculated to be 33.8 nm. Since the particle sizes are significantly smaller than the exciton Bohr radius, a large blue shift of the absorption edge is observed.

Bulk In_2S_3 is normally not luminescent at room temperature.[9] Recent observations on In_2S_3 micron-sized powders show a strong emission peaking at about 595 nm at 80 K.[17] In the particles reported here, strong blue and green luminescence is observed. In semiconductors, the most common types of emission are from exciton-like transitions and free-to-bound and donor−acceptor pair transitions, often mediated at defect sites. Recently, nanoparticles of In_2S_3 have been reported to show both UV[8,9] and orange[10] luminescence. The UV luminescence has been assigned to excitonic emission[8] while the red emission has been attributed to the Indium interstitial defect, In^{3+}.[10] The indium interstitial is also a common defect emitter in In-rich $CuInS_2$ thin films.[18,19]

Generally in nanoparticles, if the emission is from an exciton or band-to-band transition, the emission wavelength maximum

TABLE 1: Absorption and Emission Wavelengths of In_2S_3 and In_2S_3:Eu^{3+} Nanoparticles in Aqueous Solution

samples	size range (nm)	absorption (nm)	excitation (nm)	emission (nm)	stokes-shift (nm)*	efficiency (%)
In_2S_3	4−5	330, 390	310, 400	510	110	1.6
$In_{1.8}Eu_{0.2}S_3$	4−5	390	310, 400	512	112	2.2
$In_{1.6}Eu_{0.4}S_3$	2−3	340	323, 363	425	62	33

*Measured from the excitation and emission spectra.

TABLE 2: Luminescence Lifetimes of In_2S_3 Nanoparticles

particle	wavelength (nm)	lifetime (ns)	amplitude ratio*
In_2S_3	500	0.4, 2.3	55
$In_{1.8}Eu_{0.2}S_3$	500	0.7, 3.7	3
$In_{1.6}Eu_{0.4}S_3$	435	0.7, 2.5	5

*Ratio of the amplitudes of the fast and slow lifetime components.

will vary with the excitation wavelength because the absorption and emission wavelengths are size-dependent.[20] Since the nanoparticle sample contains a distribution of different sized particles, the larger particles that have smaller band gaps absorb and emit at longer wavelengths relative to smaller particles in the distribution.[20] However, if the emission is from a defect or a luminescence center such as Mn^{2+} or Eu^{3+}, the emission energy is not dependent on the excitation energy because the emission energies of these transitions are not size-dependent. Figure 7 shows clearly that the green emission position and shape of the In_2S_3 nanoparticles do not vary significantly following excitation at different wavelengths. For $In_{1.8}Eu_{0.2}S_3$ nanoparticles, the green emission wavelength also remains constant following excitation at different wavelengths. However, Figure 6c shows that the peak of the blue emission of $In_{1.6}Eu_{0.4}S_3$ moves to shorter wavelengths gradually as the excitation wavelength decreases. This is typical luminescence behavior of an excitonic or band-to-band transition from a distribution of semiconductor nanoparticles.[20]

The dependences of the emission intensity and emission wavelength with the excitation power density can also provide some valuable information about the origin of the emission. As a general rule, the emission wavelength will shift toward shorter wavelengths with increasing excitation intensity if the emission is from donor−acceptor pair recombination.[18,21−24] Power density measurements on both In_2S_3 and $In_{1.6}Eu_{0.4}S_3$ nanoparticles (data not shown) show no shift in the emission wavelength with power density. Therefore, donor and acceptor pair recombination is not likely responsible for either the blue or green emission.

The measured lifetimes in all three particles show fairly similar decay times and all are at least biexponential in nature. However, the relative quantum yields of the $In_{1.6}Eu_{0.4}S_3$ particles are about a factor of 10 higher than the other samples. These particles also show the blue emission whereas the other particles show the green emission. For purely single-exponential luminescence decays, the relation

$$\phi = \tau_{obs}/\tau_{rad} \qquad (2)$$

where ϕ is the quantum yield, and τ_{obs} and τ_{rad} are the observed and radiative lifetimes, can be used to determine the radiative lifetimes. While these relations may not be rigorously true for multiexponential decays or decays fit to a distribution of lifetimes, they can still be used to gain some insight into the nature of the transitions. We note that the values for both the quantum yield and observed lifetime of the In_2S_3 nanoparticle samples presented here are quite similar to those reported by Xiong,[9] however the emission wavelength is significantly red-

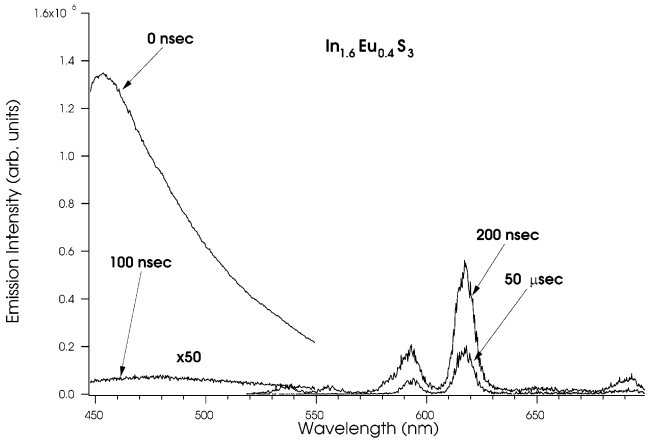

Figure 9. Time-resolved emission spectra of $In_{1.8}Eu_{0.2}S_3$ nanoparticles in aqueous solution taken at 0 ns, 100 ns, 200 ns, and 50 μs after excitation at 395 nm.

shifted. Nonetheless, it is clear from eq 2 that the $In_{1.6}Eu_{0.4}S_3$ particles have a significantly shorter radiative lifetime compared with the other particles. This is consistent with our assignment of the blue luminescence from the $In_{1.6}Eu_{0.4}S_3$ particles as a band-to-band transition and the green luminescence from the other particles as defect luminescence that would be expected to have a significantly longer lifetime. The nonradiative rate in these samples may be entirely dominated by surface trapping as is common in very small particles because of their necessarily large surface-to-volume ratio. The fast, subnanosecond decays observed may very well be associated with these trap states. We note that in the In_2S_3 pure particles, the amplitude of this component is significantly enhanced relative to the longer nanosecond decay as compared to the europium-doped particles (Table 2). Therefore, the incorporation of the Eu^{3+} ions may passivate surface defect sites as has been reported previously.[25]

Based on the luminescence behaviors described above, the blue emission from In_2S_3 nanoparticles is most likely due to excitonic recombination and the green emission is from an indium interstitial. The formation of indium interstitials in In_2S_3 is likely to occur because the particles are prepared in an acidic solution with pH 2.0 and 3.5. Under these conditions, some sulfur ions may escape as H_2S gas.

From the EDS measurements, it is clear that both manganese and europium are present in the nanoparticles as both are added during the preparation procedure, however there is no obvious spectroscopic signature for either species in the emission spectra. The luminescence from Eu^{3+} is not easily observed over the strong blue and green emission in Eu^{3+}-doped In_2S_3 nanoparticles in solution. However, red luminescence from Eu^{3+} is observed in time-resolved spectra at longer times (microseconds) once the green or blue emission from the In_2S_3 nanoparticles has decayed away. Figure 9 displays the time-resolved emission spectra taken at 0 ns, 100 ns, 200 ns, and 50 μs delay after excitation. The emission bands peaking at 579.5, 593, 615, 648, and 698 nm are from the $^5D_0-^7F_0$, $^5D_0-^7F_1$, $^5D_0-^7F_2$, $^5D_0-^7F_3$, and $^5D_0-^7F_4$ transitions of Eu^{3+}, respectively. (see Figure 11 for the details). The decay lifetime of Eu^{3+} emission in In_2S_3:

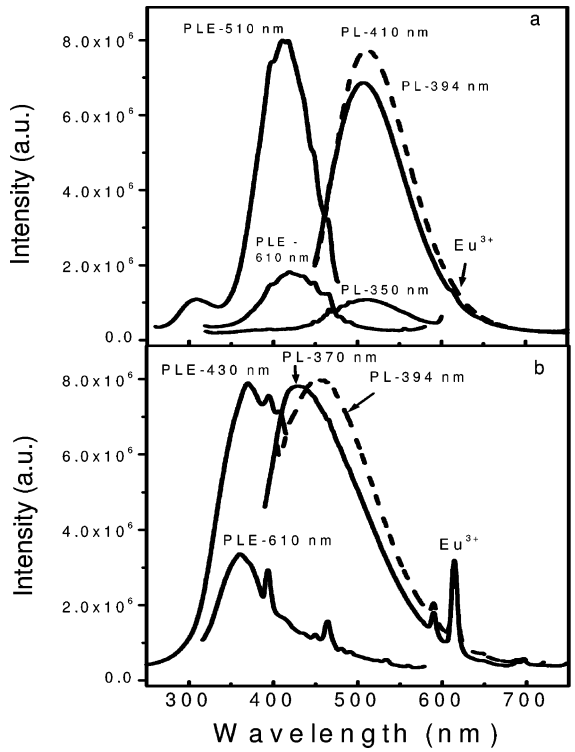

Figure 10. Excitation and emission spectra of $In_{1.8}Eu_{0.2}S_3$ and $In_{1.6}Eu_{0.4}S_3$ nanoparticle thin films. PLE-510 nm represents the photoluminescence excitation spectrum with monitored emission at 510 nm, and PL-410 nm represents the photoluminescence emission spectrum with excitation at 410 nm.

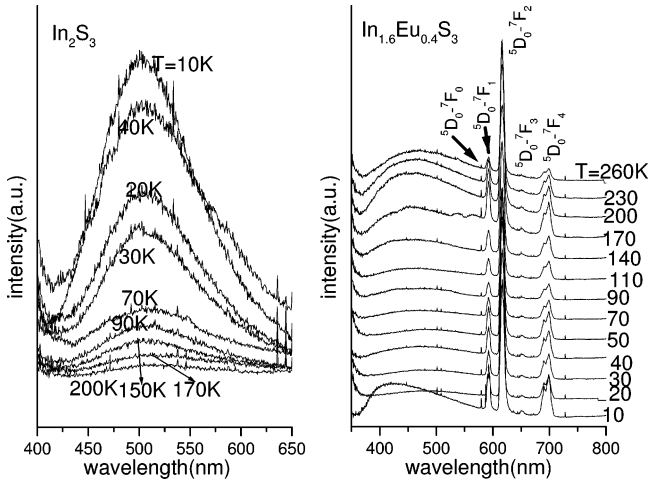

Figure 11. Emission spectra of In_2S_3 and $In_{1.6}Eu_{0.4}S_3$ nanoparticle thin films at different temperatures below room temperature. The excitation is at 325 nm.

Eu^{3+} nanoparticles is about 10 μs, much longer than either the blue or green emissions from In_2S_3. In aqueous solutions, the Eu^{3+} lifetime is significantly shortened due to quenching by energy transfer to the O−H stretch[26] of nearby water molecules.

No emission from Mn^{2+} is observed however, despite the fact that its lifetime should be in the millisecond range. Surface-adsorbed Mn^{2+} on ZnS[27] or CdS[28] nanoparticles is not luminescent, while Mn^{2+} doped into the lattice displays characteristic broad orange luminescence. Due to the difference in charge, it is unlikely that the Mn^{2+} can easily substitute for the indium in the lattice, thus the most likely place for manganese to reside is on the surfaces of the nanoparticles. Recent reports indicate that ion doping can inhibit nanoparticle growth and passivate the surface defect sites.[25,29,30] In addition, in CdS:Mn^{2+}-doped nanoparticles, the luminescence is predominantly from Mn^{2+} ions that are doped inside the particles. The Mn^{2+} species adsorbed to the nanoparticle surfaces are not luminescent.[28] In other words, the dopant ions within the lattice are responsible for emission while the ions adsorbed on the particle surfaces provide surface passivation. Likewise, some Eu^{3+} most likely resides on the surfaces of the nanoparticles, also offering surface passivation. Evidence for this can be observed as the $In_{1.8}Eu_{0.2}S_3$ sample begins to show a blue excitonic peak in the emission (Figure 6) and the higher-doped $In_{1.6}Eu_{1.6}S_3$ particles show predominantly excitonic emission. This is likely because Eu^{3+} ions first passivate the surface so that the exciton does not trap easily to the surface states. Higher Eu^{3+} doping may also replace or reduce the In^{3+} interstitial defects, resulting in purely excitonic emission with higher quantum efficiency. Strong quantum size confinement and good surface passivation probably lead to the high luminescence efficiency from $In_{1.6}Eu_{0.4}S_3$ nanoparticles.

4.2. Luminescence and Temperature Dependence of Indium Sulfide Nanoparticles Thin Films. To fabricate devices that require full-color emission properties, it is desirable to have red emission in addition to the blue and green emission of the In_2S_3 nanoparticles. Eu^{3+} is a common dopant resulting in red emission and used in fluorescent lighting and displays. In addition, solids or thin film materials that can withstand elevated temperatures may be required for some applications. Figure 10 shows the excitation and emission spectra of $In_{1.8}Eu_{0.2}S_3$ and $In_{1.6}Eu_{0.4}S_3$ nanoparticle thin films that are made by evaporating the nanoparticle solutions on glass slides. In addition to the emission of In_2S_3 particles, strong luminescence from Eu^{3+} is observed in the continuous-wave emission spectra from thin films. In this case, the Eu^{3+} luminescence is not quenched by nearby water molecules so that the luminescence is significantly enhanced relative to the aqueous nanoparticles. In the excitation spectra obtained monitoring the Eu^{3+} emission at 610 nm, the f−f transitions of Eu^{3+} and the band-to-band transition of the In_2S_3 host are observed.

The changes in the emission wavelength as a function of temperature can give important information about the luminescence mechanism. Generally, if the energy levels of the emitter are coupled to the crystal field strength or chemical bond or pair distances, the emission wavelength is temperature dependent. This behavior has been observed in the band-to-band transitions and excitonic luminescence in semiconductors,[31,32] the d−d transitions of transition metal ions,[31,33,34] and the d−f transitions of rare earth ions.[31] If the transition is not strongly influenced by the crystal field strength, then its emission wavelength is temperature independent, as observed in the f−f transitions of trivalent rare earth ions,[14,31] and some interstitial defects.[35,36] Figure 11 displays the emission of both In_2S_3 and $In_{1.6}Eu_{0.4}S_3$ thin films at different temperatures. The results shown in Figure 11 demonstrate that the 510-nm green emission peak and the red emission from Eu^{3+} do not change in emission wavelength while the 425-nm blue emission peak shifts to longer wavelengths (lower energies) at higher temperatures. The red shift of the blue emission with increasing temperature is a typical temperature behavior of excitonic emission in semiconductors[37] and supports our previous assignment. As the interstitial ions are likely at the surfaces or interfaces among the nanocrystals, the crystal field has little effect on its energy levels. This is likely why the green emission wavelength does not change with temperature.

The measurement of the luminescence intensity temperature dependence can also provide useful information about the

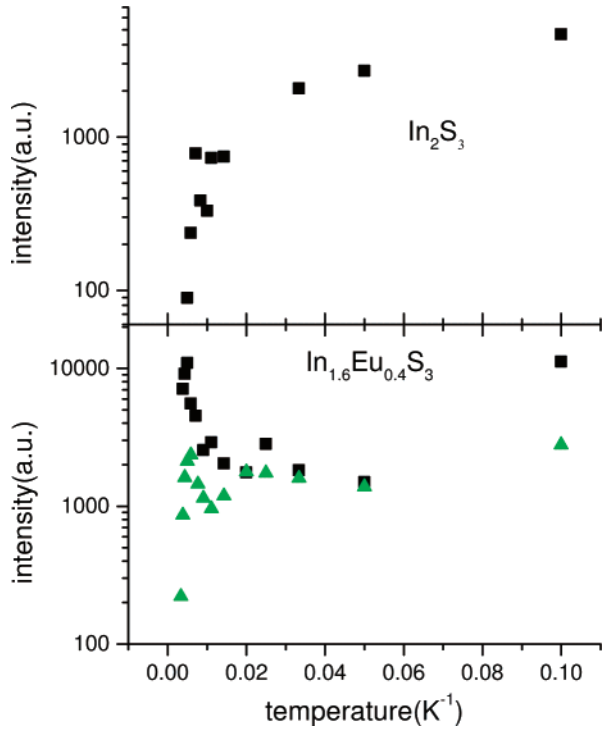

Figure 12. The emission intensity changes of In_2S_3 (upper) and $In_{1.6}Eu_{0.4}S_3$ (lower, squares for the blue emission and triangles for the red emission of Eu^{3+} at 612 nm) nanoparticle thin films at different temperatures below room temperature. The excitation is at 325 nm.

stability of the particles as well as the photophysical origins of the luminescence. Figure 12 shows the change in intensity at different temperatures below room temperature for both In_2S_3 and $In_{1.6}Eu_{0.4}S_3$ thin films. Overall, the green emission from In_2S_3 increases in intensity with decreasing temperature. However, the intensity temperature dependence of the blue emission from $In_{1.6}Eu_{0.4}S_3$ is complex, decreasing from room temperature to 20 K, while increasing at 10 K. The complex relationship between the intensity of the blue emission with temperature may be partly due to energy transfer to Eu^{3+} in $In_{1.6}Eu_{0.4}S_3$ nanoparticles. Energy transfer from the blue band to Eu^{3+} ions may occur because the blue emission band overlaps with the absorption peaks of Eu^{3+}. In this case, the intensity change of the blue emission with temperature is related to both the phonon induced nonradiative rate and the energy transfer rate. Generally, the phonon-induced nonradiative rate decreases with decreasing temperature, so the radiative emission should increase at lower temperatures. However, the energy transfer rate is enhanced at lower temperatures because the distance between the two centers becomes smaller. As a result, the blue emission intensity decreases at lower temperatures likely due to increase of energy transfer to the Eu^{3+} ions. In addition, the carriers can transfer between the energy levels responsible for the blue and red emissions. The occupation of the carriers on the higher energy level (responsible to the blue emission) will decrease with decreasing temperature, which results in the decrease of the intensity of the blue band. Therefore, the combination of phonon-induced quenching and energy transfer leads to the complex dependence of the blue emission intensity with temperature. For the emission of Eu^{3+}, both the changes in the phonon-induced nonradiative rate and the energy transfer rate enhance its intensity at lower temperatures. Therefore, the luminescence of Eu^{3+} increases in intensity with decreasing temperature.

Luminescence intensities of $In_{1.8}Eu_{0.2}S_3$ and $In_{1.6}Eu_{0.4}S_3$ nanoparticle thin films at different temperatures above room temperature show a gradual decrease with increasing temperature likely due to thermal quenching (data not shown), although strong luminescence is observed at temperatures up to 100 °C. This indicates that the particles and luminescence properties are quite stable in air, even at elevated temperatures. Eu^{3+}-doped phosphors are widely used in lighting and displays and the f−f emission of Eu^{3+} is very stable due to shielding from outer-shell electrons.[31,35] The blue and green emissions are comparable in stability to the Eu^{3+} emission, therefore these nanoparticles may make good multicolor luminescent materials.

The blue, green, and red emissions from In_2S_3 and In_2S_3:Eu^{3+} nanoparticles make them a potentially new type of full-color phosphor. In fact, both the blue and green broad emission bands cover a large portion of the full visible spectrum from the blue to red wavelength ranges. In addition, the luminescence decay lifetime is very fast and In_2S_3 nanoparticles are relatively simple to prepare. Thus, In_2S_3-based nanophosphors may have a bright future for full-color emission, flat panel displays, and lighting.

5. Conclusions

In_2S_3 and In_2S_3:Eu^{3+} nanoparticles prepared by solution techniques show blue, green, and red emission. Experimental observations on the luminescence responses following changes in the excitation wavelength and excitation power density, as well as the luminescence lifetime decays and temperature dependences, indicate that the blue emission of In_2S_3 nanoparticles is due to exciton recombination and the green emission to indium interstitial defects. The full-color emission, short luminescence decays, and good stability make In_2S_3 nanoparticles a new type of promising phosphor for flat-panel displays, lighting, and optical communications.

Acknowledgment. W. C. and S. P. W. would like to thank Nomadics, Inc., United States, the National Science Foundation (NSF, Grant No. DMI-0132030), National Institutes of Health (NIH, Grant No. 1R43CA94403-1), and the Department of Energy (DOE, DE-FG02-04ER84023) for grants. Part of the research described in this paper was performed at the W.R. Wiley Environmental Molecular Sciences Laboratory, a national scientific user facility sponsored by the Department of Energy's Office of Biological and Environmental Research and located at the Pacific Northwest National Laboratory (PNNL). PNNL is operated by Battelle for the U.S. Department of Energy under contract DE-AC06-76RLO1830. J.-O. B. would like to thank the Swedish Research Council for support. F. S. and G. L. would like to thank the National Natural Science Foundation of China for financial support (contract No. 60076012).

References and Notes

(1) Justel, T, H.; Nikol, H.; Ronda, C. *Angew. Chem., Int. Ed.* **1998**, *37*, 3084.

(2) Ekimov, A. I.; Efros, A. L.; Onuschenko A. A. *Solid State Commun.* **1985**, *56*, 921.

(3) Chen, W.; Sammynaiken, R.; Huang, Y. *J. Appl. Phys.* **2000**, *88*, 5188.

(4) (a)Knox, R. S. In *Theory of Excitons, Solid State Physics Supplements*; Academic Press: New York, 1963. (b) Curthbert, J. D.; Thomas, D. G. *Phys. Rev.* **1967**, *154*, 763.

(5) Chen, W.; Joly, A. G.; Wang, S. P. Luminescence of Semiconductor Nanoparticles. In *The Encyclopedia of Nanoscience and Nanotechnology*; Nalwa, H. S., Ed.; American Scientific Publishers: Los Angeles, 2004; Vol. 4, pp 689−718.

(6) Alivisatos, A. P. *J. Phys. Chem.* **1996**, *100*, 13226.

(7) Kamat, P. V.; Dimitrijevic, N. M.; Fessenden, R. W. *J. Phys. Chem*. **1988**, *92*, 2324.
(8) Nagesha, D. K.; Liang, X. R.; Mamodov, A.; Gainer, G.; Eastman, M. A.; Giersig, M.; Song, J.; Kotov, N. A. *J. Phys. Chem. B* **2001**, *105*, 7490.
(9) Xiong, Y. J.; Xie, Y.; Du, G. A.; Tian X. B.; Qian, Y. T. *J. Solid State Chem*. **2002**, *166*, 336.
(10) Ai, Z. P. *Opt. Mater*. **2003**, *24*, 589.
(11) Avivi, S.; Palchick, O.; Palchik, V.; Slifkin, M. A.; Weiss, A. M.; Gedanken, A. *Chem. Mater*. **2001**, *13*, 2195.
(12) Yasaki, Y.; Sonoyama, N.; Sakata, T. *J. Electroanal. Chem*. **1999**, *469*, 116.
(13) Rooymans, C. J. M. *J. Inorg. Nucl. Chem*. **1959**, *4*, 119.
(14) Chen, W.; Joly, A. G.; Kowalchuk, M. C.; Malm, J.-O.; Huang, Y.; Bovin, J.-O. *J. Phys. Chem. B* **2002**, *106*, 7034.
(15) Hara, K.; Sayama, K.; Arakawa, H. *Sol. Energy Mater. Sol Cells* **2000**, *62*, 441.
(16) Kim, W. T.; Kim, C. D. *J. Appl. Phys*. **1986**, *60*, 2631.
(17) Gorai, S.; Guha, P.; Ganguli, D.; Chaudhuri, S. *Mater. Chem. Phys.* **2003**, *82*, 974.
(18) Binsma, J. M.; Giling, L. J.; Bloem, J. *J. Lumin*. **1982**, *27*, 36.
(19) Wijesundara, R.; Siripala, W. *Sol. Energy Mater. Sol Cells* **2004**, *81*, 147.
(20) Hoheisel, W.; Colvin, V. L.; Johnson, C. S.; Alivisatos, A. P. *J. Chem. Phys*. **1994**, *101*, 8455.
(21) Thomas, D. G.; Hopfield, J. J.; Augustiniak, W. M. *Phys. Rev. B* **1965**, *140*, 202.
(22) Lahlou, N.; Masse, G. *J. Appl. Phys*. **1981**, *52*, 978.
(23) Chang, Y.; Chu, J. H.; Tang, W. G.; Shen, W. Z.; Tang, D. Y. *IR Phys. Technol*. **1996**, *37*, 747.
(24) Topper, K.; Bruns, J.; Scheer, R.; Weber, M.; Weidinger, A.; Braunig, D. *Appl. Phys. Lett*. **1997**, *71*, 482.
(25) Pires, A. M.; Santos, M. F.; Davolos, M. M. R.; Stucchim, E. B. *J. Alloys Compd.* **2002**, *344*, 276.
(26) Bartlett, J.; Cooney, R. P.; Kydd, R. A. *J. Catal*. **1988**, *114*, 58.
(27) Sooklal, K.; Cullum, B. S.; Angel, S. M.; Murphy, C. J. *J. Phys. Chem.* **1996**, *100*, 4551.
(28) Counio, G.; Esnouf, S.; Gacoin, T.; Biolot, J.-P. *J. Phys. Chem*. **1996**, *100*, 20021.
(29) Han, J. P.; Mantas, P. Q.; Senos, A. M. R. *J. Mater. Res*. **2001**, *16*, 459.
(30) Logan, R. A.; Schumaker, N. E.; Henry, C. H.; Merritt, F. R. *J. Appl. Phys*. **1979**, *50*, 5970.
(31) Wang, S. P.; Westcott, S. L.; Chen, W. *J. Phys. Chem. B* **2002**, *106*, 11203.
(32) Hunter, A. T.; McGill, T. C. *J. Appl. Phys.* **1981**, *52*, 5779.
(33) Tanaka, M.; Masumoto, Y. *Chem. Phys. Lett*. **2000**, *324*, 249.
(34) Chen, W.; Su, F.; Li, G. H.; Joly, A. G.; Malm, J.-O.; Bovin, J.-O. *J. Appl. Phys*. **2002**, *92*, 1950.
(35) Grattan, K. T. V.; Zhang, Z. Y. *Fiber Optic Fluorescence Thermometry*; Chapman and Hall: London, 1995.
(36) Halliday, D. P.; Potter, M. D. G.; Mullins, J. T.; Brinkman, A. W. *J. Cryst. Growth* **2000**, *220*, 30.
(37) Moss, T. S. *Optical Properties of Semiconductors*; Butterworth Scientific Publications: London, 1959.